

# Bioinformatic and biochemical analysis of the key binding sites of the pheromone binding protein of *Cyrtotrachelus buqueti* Guerin-Meneville (Coleoptera: Curculionidea)

Hua Yang<sup>Equal first author, 1</sup>, Yan-Lin Liu<sup>Equal first author, 1</sup>, Yuan-Yuan Tao<sup>1</sup>, Wei Yang<sup>Corresp., 1</sup>, Chun-Ping Yang<sup>1</sup>, Jing Zhang<sup>2</sup>, Li-Zhi Qian<sup>1</sup>, Hao Liu<sup>1</sup>, Zhi-Yong Wang<sup>3</sup>

<sup>1</sup> Sichuan Agricultural University, Key Laboratory of Ecological Forestry Engineering of Sichuan Province/College of Forestry, Chengdu, Sichuan, China

<sup>2</sup> Provincial Key Laboratory of Agricultural Environmental Engineering, Sichuan Agricultural University, Chengdu, China

<sup>3</sup> Key Laboratory of Control and Resource Development of Bamboo Pest of Sichuan Province, Leshan, China

Corresponding Author: Wei Yang

Email address: ywei0218@aliyun.com

The bamboo snout beetle *Cyrtotrachelus buqueti* is a widely distributed wood-boring pest found in China, and its larvae cause significant economic losses because this beetle targets a wide range of host plants. A potential pest management measure of this beetle involves regulating olfactory chemoreceptors. In the process of olfactory recognition, pheromone-binding proteins (PBPs) play an important role. Homology modeling and molecular docking were conducted in this study for the interaction between CbuqPBP1 and dibutyl phthalate to better understand the relationship between PBP structures and their ligands. Site-directed mutagenesis and binding experiments were combined to identify the binding sites of CbuqPBP1 and to explore its ligand-binding mechanism. The 3D structural model of CbuqPBP1 has six  $\alpha$ -helices. Five of these  $\alpha$ -helices adopt an antiparallel arrangement to form an internal ligand-binding pocket. When docking dibutyl phthalate within the active site of CbuqPBP1, a CH- $\pi$  interaction between the benzene ring of dibutyl phthalate and Phe69 was observed, and a weak hydrogen bond formed between the ester carbonyl oxygen and His53. Thus, Phe69 and His53 are predicted to be important residues of CbuqPBP1 involved in ligand recognition. Site-directed mutagenesis and fluorescence assays with a His53Ala CbuqPBP1 mutant showed no affinity toward ligands. Mutation of Phe69 only affected binding of CbuqPBP1 to cedar camphor. Thus, His53(Between  $\alpha$ 2 and  $\alpha$ 3) of CbuqPBP1 appears to be a key binding site residue, and Phe69(Located at  $\alpha$ 3) is a very important binding site for particular ligand interactions.

1     **Bioinformatic and biochemical analysis of the key binding sites of the**  
2 **pheromone binding protein of *Cyrtotrachelus buqueti* Guerin-Meneville**  
3 **(Coleoptera: Curculionidea)**

4 Hua Yang<sup>1¶</sup>, Yan-Lin Liu<sup>1¶</sup>, Yuan-Yuan Tao<sup>1¶</sup>, Wei Yang<sup>1\*</sup>, Chun-Ping Yang<sup>1</sup>, Jing Zhang<sup>2</sup>, Li-  
5 Zhi Qian<sup>1</sup>, Hao Liu<sup>1</sup> and Zhi-Yong Wang<sup>3</sup>

6

7     <sup>1</sup> Key Laboratory of Ecological Forestry Engineering of Sichuan Province, College of Forestry,  
8 Sichuan Agricultural University, Chengdu, Sichuan 611130, China.

9     <sup>2</sup> Provincial Key Laboratory of Agricultural Environmental Engineering, Sichuan Agricultural  
10 University, Chengdu, Sichuan 611130, China.

11     <sup>3</sup> Key Laboratory of Control and Resource Development of Bamboo Pest of Sichuan Province,  
12 Leshan, Sichuan, 614000, China.

13

14     \*Corresponding Author:

15     Wei Yang

16     E-mail: [ywei0218@aliyun.com](mailto:ywei0218@aliyun.com)

17     ¶These authors contributed equally to this article



**19 Abstract**

20 The bamboo snout beetle *Cyrtotrachelus buqueti* is a widely distributed wood-boring pest found  
21 in China, and its larvae cause significant economic losses because this beetle targets a wide range  
22 of host plants. A potential pest management measure of this beetle involves regulating olfactory  
23 chemoreceptors. In the process of olfactory recognition, pheromone-binding proteins (PBPs)  
24 play an important role. Homology modeling and molecular docking were conducted in this study  
25 for the interaction between CbuqPBP1 and dibutyl phthalate to better understand the relationship  
26 between PBP structures and their ligands. Site-directed mutagenesis and binding experiments  
27 were combined to identify the binding sites of CbuqPBP1 and to explore its ligand-binding  
28 mechanism. The 3D structural model of CbuqPBP1 has six  $\alpha$ -helices. Five of these  $\alpha$ -helices  
29 adopt an antiparallel arrangement to form an internal ligand-binding pocket. When docking  
30 dibutyl phthalate within the active site of CbuqPBP1, a CH- $\pi$  interaction between the benzene  
31 ring of dibutyl phthalate and Phe69 was observed, and a weak hydrogen bond formed between  
32 the ester carbonyl oxygen and His53. Thus, Phe69 and His53 are predicted to be important  
33 residues of CbuqPBP1 involved in ligand recognition. Site-directed mutagenesis and  
34 fluorescence assays with a His53Ala CbuqPBP1 mutant showed no affinity toward ligands.  
35 Mutation of Phe69 only affected binding of CbuqPBP1 to cedar camphor. Thus, His53(Between  
36  $\alpha$ 2 and  $\alpha$ 3) of CbuqPBP1 appears to be a key binding site residue, and Phe69(Located at  $\alpha$ 3) is a  
37 very important binding site for particular ligand interactions.

38 **Keywords:** *Cyrtotrachelus buqueti*, pheromone binding protein, bioinformatics, site-directed

39 mutagenesis, fluorescence assay

40

## 41 Introduction

42 During long-term evolution insects have developed a sensitive sense of smell, which enables  
43 insects to detect external volatile semiochemicals when searching for various environmental cues,  
44 such as foraging for food, finding a breeding partner and locating a spawning ground(Gu *et al.*,  
45 2011; Larsson *et al.*, 2004). Tentacles are the main olfactory part of insects and contain a large  
46 variety of receptors. Receptors are widely distributed with various olfactory-rated functional  
47 proteins, including odorant binding proteins (OBPs), chemosensory proteins (CSPs) and  
48 olfactory receptors (Ors). OBPs are divided into pheromone binding proteins (PBPs), general  
49 odorant binding proteins (GOBPs) and antennal binding proteins (ABPs)(Vogt and Riddiford  
50 1981). Research on the binding mechanism between OBPs and ligand molecules has been a  
51 major focus of research, including defining the three-dimensional (3D) structure of these OBPs.  
52 Kruse *et al.*, (2003) and Thode *et al.*, (2008) initially analyzed the general odorant binding  
53 protein (LUSH) of *Drosophila melanogaster* and the crystal structure of the complex between  
54 LUSH and alcohol, and clarified that Thr57 is a key residue involved in ligand interaction. In  
55 accordance with X-ray diffraction analysis of the pheromone binding protein BmorPBP of  
56 *Bombyx mori* and structure of bombykol, Sandler *et al.* (2000) discovered that Ser56 of this  
57 protein played a key role by forming a hydrogen bond with the ligand bombykol. According to  
58 the structures of odorant binding protein CquiOBP1 and MOP of *Culex quinquefasciatus*, Mao *et*  
59 *al.* (2010) discovered that instead of hydrogen bonds, the interaction between protein and ligand  
60 was driven by van der Waals forces and hydrophobic interactions. Based on the structure

61 between the odorant binding protein HoblOBP2 of *Holotrichia oblita* and ethyl  
62 benzenecarboxylate, Zhuang *et al.* (2013) discovered that this protein-ligand complex involved  
63 both van der Waals forces and hydrophobic interactions. Currently, high-resolution structural  
64 data describing the complex between the pheromone binding protein of *Cyrtotrachelus buqueti*  
65 and an odor molecule is unavailable, and thus information about the mode of action of this  
66 protein remains unresolved.

67 *Cyrtotrachelus buqueti* (*C. buqueti*) also named as the bamboo snout beetle, belongs to  
68 *Cyrtotrachelus*, Curculionidea, Coleoptera. *C. buqueti* is endangering survival of bamboo shoots  
69 from 28 different types of bamboos, including *Bambusa*, *Dendrocalamopsis* and *Dendrocalamus*.  
70 In particular, the larvae prefer the bamboo shoots of *Phyllostachys pubescens*,  
71 *Dendrocalamopsis oldhami*, *Bambusa textilis*, *Bambusa pervariabilis*, *Dendrocalamopsis daii*  
72 and other sympodial bamboo species(Ju *et al.*, 2005; Wang *et al.*, 2005). *C. buqueti* is distributed  
73 widely in the Sichuan Province, Chongqing City, Guangdong Province, Guangxi Province,  
74 Guizhou Province and other provinces (districts) as well as Vietnam, Burma, Thailand and other  
75 countries and regions in Southeast Asia(Yang *et al.*, 2009). *C. buqueti* is one of 233 hazardous  
76 forest pests issued in 2003 for the first time(Yang *et al.*, 2015).

77 Currently, research on *C. buqueti* has mainly concentrated on a description of the general  
78 biological characteristics and common chemical pest control approaches(Ju *et al.*, 2005; Wang *et*  
79 *al.*, 2005; Yang *et al.*, 2010; Yang *et al.*, 2009). The development of sex attractants remains  
80 poorly understood. Mang *et al.* (2012) have extracted and studied the body surface

81 semiochemicals of *C. buqueti* adults, whereas Yang *et al.* (2017a) have constructed a  
82 transcriptome library of *C. buqueti* and analyzed the sex pheromone binding protein gene. Yang  
83 *et al.* (2017b) have also cloned the sex pheromone binding protein gene that codes for the protein  
84 CbuqPBP1, and conducted fluorescence competitive binding assays for many types of simple  
85 odor substances. According to the system evolutionary tree, CbuqPBP1 was quite similar to  
86 PBP of other insects. Amino acid sequence similarity analysis showed that CbuqPBP1 had  
87 37.68% similarity with 27 PBPs of 17 insects of Coleoptera and Lepidoptera. The similarities  
88 with Coleoptera and Lepidoptera were 38.47% and 52.39% respectively (Yang *et al.*, 2018).

89 In this paper, homology modeling of the pheromone binding protein CbuqPBP1 of *C.*  
90 *buqueti* has been conducted to create a 3D model of the protein. Molecular docking has also been  
91 carried out to define the interaction mode between the ligand dibutyl phthalate and CbuqPBP1.  
92 Two key binding site residues, Phe69 and His53, were identified from this modeling and were  
93 mutated. Fluorescence competitive binding assays were conducted for these mutants and binding  
94 mechanism between CbuqPBP1 and odor molecules was analyzed. The results provide a  
95 platform for using pheromones to prevent and control *C. buqueti* efficiently.

96

## 97 **Materials & Methods**

### 98 **Materials**

99 Three compounds were chosen to investigate the ligand-binding specificity of CbuqPBP1.

100 Ligands of the highest purity were purchased from Aladdin (Shanghai, China) and stored in  
101 accordance with the manufacture's specifications. The sequence of CbuqPBP1 was taken from  
102 the GenBank with accession number KU845733.1.

### 103 **Alignment and homology modeling**

104 The amino acid sequence of CbuqPBP1 was downloaded from the GenBank and Blast was used  
105 to search against the CbuqPBP1 protein sequence in the Protein Data Bank to identify a  
106 structural template. Software Modeller 9.19 (<http://salilab.org/modeller/>) was used for homology  
107 modeling based on the sequence comparison results with the structural template sequence  
108 identified. The 3D structure obtained from modeling was evaluated with SAVES v5.0  
109 (<https://servicesn.mbi.ucla.edu/SAVES/>). After confirming the models, the Chiron  
110 (<http://redshift.med.unc.edu/chiron/login.php>) on-line server was used for optimization. Modeller  
111 9.19 was used to optimize loop regions and PyMOL was used to analyze structural  
112 characteristics and to search for ligand binding sites.

### 113 **Molecular docking**

114 Based on the established homology model, the docking program AUTODOCK vina 1.1.2 was  
115 used to find the potential binding mode between CbuqPBP1 and the ligand dibutyl phthalate.  
116 Dibutyl phthalate with strong affinity is a female pheromone of the giant bamboo weevil, which  
117 plays a role in the process of male individual searching for female individual. ChemBioDraw  
118 Ultra 14.0 was used to simulate the structure of dibutyl phthalate and to generate a 3D structure

119 of the ligand. Energy optimization was conducted using the MMFF94 force field and Autodock  
120 Tools 1.5.6 was used to create the PDBQT format(Huey *et al.*, 2007; Morris *et al.*, 2009).  
121 Binding coordinates of CbuqPBP1 and dibutyl phthalate were set to: center\_x = 22.389, center\_y  
122 = -25.143, center\_z = 1.08, and size\_x = 15, size\_y = 15, size\_z = 15. Parameter exhaustiveness  
123 was set to 20 and default values were used for other parameters to increase the calculation  
124 accuracy. Finally, the conformation with the highest score was selected and PyMoL 1.7.6 was  
125 used for visual inspection and analysis of the structural data.

### 126 **Site-directed mutagenesis**

127 The CbuqPBP1 coding sequence was mutated to yield the two mutants CbuqPBP1-Phe69A  
128 (phenylalanine to alanine at position 69) and CbuqPBP1-His53A (histidine to alanine at position  
129 53). PCR reactions were used to form overlapping chains. The extension of overlapping chains  
130 was used to splice segments in a superimposed manner. Primer5 was used to design primers  
131 (Table 1). Three rounds of PCR amplification were conducted after designing primers.  
132 Expression vectors (pET-28a(+)/PBP1-Phe69A, pET-28a(+)/PBP1-His53A and pET-  
133 28a(+)/PBP1) were generated and transformed into *Escherichia coli* BL21(DE3) competent cells  
134 for protein overexpression. Recombinant proteins produced were detected by SDS-PAGE  
135 analysis.

### 136 **Expression and purification of the native protein and mutants**

137 Expression plasmids were transformed into *E. coli* TOP10 competent cell and plated on agar

138 plates. Several colonies were selected randomly for overnight cultivation in LB media and  
139 plasmids were extracted for sequencing. Mutant plasmids pET-28a(+)/PBP1- Phe69A and pET-  
140 28a(+)/PBP1- His53A with the correct sequence were transformed into *E. coli* BL21(DE3)  
141 competent cells, and cells were grown to an optical density at 600 nm ( $OD_{600}$ ) of 0.6. IPTG was  
142 added to the culture to a final concentration of 1 mM and cells were further grown at 37 °C with  
143 shaking for 3 h to induce protein expression(Deng *et al.*, 2011). After harvesting cells by  
144 centrifugation, ultrasound sonication was used to disrupt cells (200 W, 3/4 s, 25–30 min). The  
145 supernatants and sediments were collected under low temperature centrifugation (16000 g-force,  
146 50 min) and SDS-PAGE detection was conducted. Nickel affinity (Ni-NTA) was used to purify  
147 recombination proteins, and the purified proteins were stored in Tris-HCl buffer (pH 7.4, 50  
148 mM). To avoid the function of the protein being affected by the His-tag, recombinant bovine  
149 enterokinase was used to remove the His-tag and the protein was re-purified and collected. Purity  
150 was confirmed by SDS-PAGE analysis.

### 151 **Fluorescence assay**

152 To measure the affinity of the fluorescent ligand N-phenyl-1-naphthylamine (1-NPN) toward  
153 CbuqPBP1, a 2  $\mu$ M solution of protein in 50 mM Tris-HCl, pH 7.4, was titrated with aliquots of  
154 1 mM 1-NPN dissolved in methanol to a final concentration of 16  $\mu$ M. The probe was excited at  
155 337 nm and emission spectra were recorded between 350 and 550 nm. To evaluate the effect of  
156 pH on the binding affinity of CbuqPBP1, we also measured its binding with 1-NPN over a pH  
157 range of 4.5–9.0. The displacement of 1-NPN by selected ligands was measured in a competitive

158 binding assay using both the protein and 1-NPN at 2  $\mu$ M. The mixtures were titrated with 1 mM  
159 methanol solutions of each competitor at concentrations of 2–16  $\mu$ M. The fluorescence of the  
160 mixture was recorded after 5 min. Dissociation constants for 1-NPN and the stoichiometry of  
161 binding were obtained from Scatchard plots of the binding data using the Prism software. For  
162 other competitor ligands, the dissociation constants were calculated from the corresponding half  
163 maximal inhibitory concentration ( $IC_{50}$ ) values using the equation: inhibitory constant  $K_i =$   
164  $[IC_{50}]/(1 + [1-NPN]/K_{1-NPN})$ , where [1-NPN] is the free concentration of 1-NPN and  $K_{1-NPN}$  is the  
165 dissociation constant of the protein/1-NPN complex.

166

## 167 **Results**

### 168 **Three-dimensional model of CbuqPBP1**

169 On the basis of the Blast search against the Protein Data Bank, two types of insect odor proteins  
170 with known structures and quite similar sequences to the CbuqPBP1 sequence were found. These  
171 two odorant binding proteins were *Nasonovia ribisnigri* OBP3 (NribOBP3 PDB ID: 4Z45\_A)  
172 and *Megoura viciae* OBP3 (MvicOBP3 PDB ID: 4Z39\_A). The total sequence identity between  
173 the target (CbuqPBP1) and the template protein (NribOBP3) is 33% (Cavasotto and Phatak  
174 2009)(Fig. 1A). The resolution of the template is 2.02 Å.

175 After homology modeling, the 3D structure of CbuqPBP1 (Fig. 1B) is clearly very similar  
176 to the 3D structure of the template NribOBP3 (Fig. 1C). The structural characteristics of

177 CbuqPBP1 are similar to other sex pheromone binding proteins and include six  $\alpha$ -helices:  
178 residues 26–36 ( $\alpha$ 1), 44–51 ( $\alpha$ 2), 59–72 ( $\alpha$ 3), 83–94 ( $\alpha$ 4), 101–114 ( $\alpha$ 5) and 123–137 ( $\alpha$ 6). Six  
179 conserved cysteine residues stabilize the protein structure by forming three disulfide bonds.  
180 Disulfide bond Cys36–Cys67 connects  $\alpha$ 1 and  $\alpha$ 3, Cys63–Cys121 connects  $\alpha$ 3 and  $\alpha$ 6, and  
181 Cys110–Cys130 connects  $\alpha$ 5 and  $\alpha$ 6. Five of the  $\alpha$ -helices adopt an antiparallel arrangement  
182 ( $\alpha$ 1,  $\alpha$ 3,  $\alpha$ 4,  $\alpha$ 5 and  $\alpha$ 6) and form an internal binding pocket.  $\alpha$ 2 forms a cover-type structure or  
183 lid above the pocket, which stabilizes this structure.

184 The result of further rationality estimates by Pro-CHECK (Fig. 1D) was that 88.4% residues  
185 were in the favored regions (red area A, B and L), 10.1% of the residues fall into additionally  
186 allowed regions (bright yellow area a, b, l, p) and 0.8% residues have backbone torsion angles  
187 that fall into generously allowed regions (light yellow area  $\sim$ a,  $\sim$ b,  $\sim$ l,  $\sim$ p). The percentage sum  
188 of residues in the allowed regions was 99.3%, which was higher than 95%. This result showed  
189 that the constructed 3D structure of CbuqPBP1 was a high-quality model.

190 Energy assessment was performed on ProSa (Fig. 1E). The shadow part is Z-score value  
191 of all proteins similar to Cbuq PBP1 protein in PDB database, and the black spot is Z-score value  
192 of Cbuq PBP1 protein, which is -4.35. The Z-score value of template protein NOBP3 is -5.87 in  
193 the range of Z-score of known reasonable structural proteins, which indicates that the modeling  
194 structure is more stable than template structure. This indicates that the homologous modeling  
195 Institute is more stable than template structure. The constructed CBUq PBP1 protein is  
196 reasonable in energy.

## 197 **Molecular docking**

198 To research characteristics of CbuqPBP1 binding with odor molecules, dibutyl phthalate  
199 (Fig. 2A), which interacts with CbuqPBP1 favorably, was selected to construct a complex  
200 between CbuqPBP1 3D model and dibutyl phthalate. Such a model should clarify the mode of  
201 interaction of dibutyl phthalate with CbuqPBP1 at the molecular level. We have docked dibutyl  
202 phthalate with the active pocket of CbuqPBP1, with a binding energy of  $-6.4$  kcal/mol.  
203 Generally, compound dibutyl phthalate bound to the active pocket of CbuqPBP1 with a compact  
204 conformation (Fig. 2B).

205 The benzene ring and one aliphatic chain of dibutyl phthalate were located in the  
206 hydrophobic region at the bottom of the pocket. Strong hydrophobic interactions formed between  
207 the ligand and residues Leu3, Leu4, Leu5, Leu29, Leu50, Pro56, Ile65 and Phe69. Another side  
208 chain of dibutyl phthalate was located at the opening of the pocket. Based on detailed analysis, a  
209 CH- $\pi$  interaction may occur between the benzene ring of dibutyl phthalate and residue Phe69.  
210 Moreover, an important long-range hydrogen bond ( $3.3$  Å) can form between one ester carbonyl  
211 oxygen of dibutyl phthalate and residue His53 (Fig. 2C). All aforementioned interactions enable  
212 the formation of a stable complex between dibutyl phthalate and CbuqPBP1.

## 213 **Site-directed mutagenesis of CbuqPBP1 and binding specificities of mutants**

214 After double enzyme digestion with restriction enzymes *Nde* I and *Xha* I, mutant plasmids pET-  
215 28a(+)/CbuqPBP1-His53A and pET-28a(+)/CbuqPBP1-Phe69A, and the original plasmid pET-

216 28a(+)/PBP1 formed bands in an agarose gel that were ~400 bp in length (Fig. 3). After SDS-  
217 PAGE analysis of protein overexpression, three specific bands with molecular weights of 16 kDa  
218 were observed in the SDS-PAGE gel, which is consistent with expected molecular weight of the  
219 target proteins (Fig. 4).

220 After ultrasonication to disrupt the bacteria and release the recombinant proteins (including  
221 His tag), SDS-PAGE analysis could be conducted (Fig. 5). All recombinant proteins were found  
222 in the supernatant part of the disrupted cells. After purification, recombinant bovine enterokinase  
223 was used to cleave the His-tag and following a further round of purification pure recombinant  
224 protein samples were obtained.

225 1-NPN was selected as the fluorescent probe. Fluorescence competitive binding assays were  
226 conducted for the purified wild-type CbuqPBP1, mutant CbuqPBP1-His53A and CbuqPBP1-  
227 Phe69A proteins. The fluorescence peak maximum in the presence of the recombinant proteins  
228 was recorded at different concentrations. The Scatchard equation was used to calculate the  
229 equilibrium binding constant ( $K_d$ ) between CbuqPBP1, CbuqPBP1-His53A, CbuqPBP1-Phe69A  
230 and 1-NPN, which were determined to be 2.725, 3.352 and 2.260  $\mu\text{M}$ , respectively. When the  
231 final concentration of odor substance was higher than 50  $\mu\text{M}$ , the fluorescence peak did not  
232 decrease to half its value. This showed that almost no affinity was established between protein  
233 and the odor substance, and the binding constant could not be calculated (Fig. 6).

234 Dibutyl phthalate, benzothiazole and cedar camphor were selected based on previous  
235 fluorescence binding assay test (Yang *et al.*, 2017b). Fluorescence competitive binding assays

236 were conducted with CbuqPBP1, CbuqPBP1-His53A and CbuqPBP1-Phe69A (Fig. 7). Based on  
237 the results, CbuqPBP1 bound favorably with dibutyl phthalate, benzothiazole and cedar camphor.  
238 The binding ability of CbuqPBP1-His53A with the three types of odor substances was essentially  
239 lost. The binding ability of CbuqPBP1-Phe69A mutant with cedar camphor was significantly  
240 reduced, whereas affinity toward the other two odor substances was not significantly different  
241 from that of the wild-type protein (Table 2).

242

## 243 Discussion

244 Currently, 3D structure prediction of odorant binding proteins through homology modeling has  
245 been conducted for proteins from *Choristoneura rosaceana*, *Choristoneura murinana*,  
246 *Pectinophora gossypiella*, *Heliothis assulta*, *Spodoptera exigua*, *Spodoptera exigua*, *Holotrichia*  
247 *oblita*, *lettuce Aphidoidea*, *Megoura viciae* and other insects(Northey *et al.*, 2016; Sun *et al.*,  
248 2013; Wang *et al.*, 2015). On the basis of homology modeling of pheromone binding protein  
249 CbuqPBP1 of *C. buqueti*, the 3D structure is composed of six  $\alpha$ -helices, which packed together  
250 and were stabilized by three disulfide bonds. Disulfide bonds Cys36–Cys67, Cys63–Cys121 and  
251 Cys110–Cys130 connected  $\alpha$ 1 and  $\alpha$ 3,  $\alpha$ 3 and  $\alpha$ 6,  $\alpha$ 5 and  $\alpha$ 6 respectively. Five of the  $\alpha$ -helices  
252 arranged in an antiparallel manner to form an internal binding pocket(Tian *et al.*, 2017).  $\alpha$ 2  
253 formed a cover-type structure above the pocket, which was similar to *Holotrichia oblita*  
254 *HoblOBP2*(Zhuang *et al.*, 2013) structures. As for 3D structure of *Bombyx mori* BmorPBP, four  
255 antiparallel  $\alpha$ -helices formed a hydrophobic pocket and  $\alpha$ 2 and  $\alpha$ 3 did not participate in the

256 formation of the pocket(Sandler *et al.*, 2000). This might be due to differences in hydrophobic  
257 pocket of the 3D structure of odorant binding proteins from different insects. Such differences  
258 are likely to be closely related to the function of these proteins.

259 According to research, odorant binding proteins from some insects interact with their cognate  
260 ligand through hydrogen bonds and hydrophobic interactions, whereas other odorant binding  
261 proteins from other insects interact with odorants via van der Waals forces and hydrophobic  
262 interactions(Sandler *et al.*, 2000). In this report, a CH- $\pi$  interaction formed between the benzene  
263 ring of dibutyl phthalate and Phe69. This CH- $\pi$  interaction is generally considered to be a  
264 relatively weak hydrogen bond. Previous research has indicated that CH- $\pi$  interactions are  
265 important in carbohydrate–protein identification processes, where the CH- $\pi$  features as a  
266 synergistic interaction that plays an important role in stabilizing the structure of the complex  
267 (Jiang *et al.*, 2009; Kozmon *et al.*, 2011). The CH- $\pi$  interaction involves a nonpolar interaction  
268 between the CH proton and electron-rich aromatic ring  $\pi$  electron cloud system, playing a similar  
269 role to hydrogen bonding in controlling crystal stacking, maintaining biomolecular structures and  
270 participating in molecular recognition processes(Ye *et al.*, 2015; Zhao *et al.*, 2014). Therefore,  
271 we hypothesize that the CH- $\pi$  interaction may play a role in binding and stabilizing the  
272 interaction with odor molecules.

273 An ester carbonyl oxygen from dibutyl phthalate and His53 from the protein formed a weak  
274 3.3 Å hydrogen bond. Such a hydrogen bond has been reported in odorant binding proteins of  
275 other insects, for example, BmorPBP1 of *B. mori* and pheromone compound interacted through a

276 hydrogen bond. General odorant binding protein (LUSH) from *Drosophila melanogaster* and the  
277 pheromone binding protein (ApolPBPI) from *Antheraea polyphemus* interact with their cognate  
278 ligands through hydrogen bonds(Damberger *et al.*, 2007; Thode *et al.*, 2008). Therefore, we  
279 hypothesized that the CbuqPBP1 interaction and release of the ligand involves hydrogen bond  
280 formation via His53.

281       According to the fluorescence competitive binding assay, mutant pET-28a(+)/PBP1-His53A  
282 could not interact with odor substances. Replacing His53 with alanine removed the ability of the  
283 mutant to form this key hydrogen bond with ligands, and therefore the ability to bind with odor  
284 substances. Thus, His53 is a key binding site residue of the pheromone binding protein of *C.*  
285 *buqueti*. Mutein pET-28a(+)/PBP1-Phe69A did not bind cedar camphor. However, only a  
286 decrease in binding ability toward dibutyl phthalate and benzothiazole was observed. These  
287 observations indicate that only a small number of intermolecular forces between the protein and  
288 odor molecules were affected by this mutation(Zhuang *et al.*, 2014). Thus, the binding affinity  
289 had been reduced, but not completely lost. Therefore, Phe69 is the binding site for CbuqPBP1 to  
290 combine with odor substance; however, Phe69 is not a key binding site residue. Moreover, these  
291 observations showed that the combination between CbuqPBP1 and ligands was affected by loss  
292 of hydrogen bonding and other intermolecular forces, and the interaction between CbuqPBP1  
293 and ligands involves the joint action of many acting forces and the binding site(Li et al. 2016).

## 294 **Acknowledgments**

295 This work was funded by the key fund of the education department in Sichuan (17ZB0344) and

296 the key laboratory fund for scientific research in Sichuan (003Z1401). The experiments were  
297 conceived and coordinated by HY, YYT, YLL, WY, ZYW ,LZQ and CPY. Sampling was  
298 performed by HY, YLL and YYT. Molecular docking was performed by HY, YLL, HL and JZ.  
299 HY, YLL and WY drafted the manuscript. All authors read and approved the final version of the  
300 manuscript submitted for publication. The authors thank Liwen Bianji, Edanz Editing China  
301 ([www.liwenbianji.cn/ac](http://www.liwenbianji.cn/ac)), for editing the English text of a draft of this manuscript.

302

303 **Figure legends**

304 **Figure 1 Three-dimensional (3D) model of CbuqPBP1.** (A) Sequence alignment between  
305 CbuqPBP1 and NribOBP3. (B) 3D structure of CbuqPBP1. The N and C termini and the six  $\alpha$ -  
306 helices are labeled and the three disulfide linkages are shown in yellow stick representations. (C)  
307 Superimposed penetrative structure of CbuqPBP1 and NribOBP3. The model of CbuqPBP1 and  
308 crystal structure of NribOBP3 are shown in green and violet, respectively. (D) The results of the  
309 PROCHECK evaluation of the CbuqPBP1 model. (E) Overall model quality.

310 **Figure 2 The binding pocket of CbuqPBP1 and the docking result with dibutyl phthalate.**  
311 (A) Tertiary structure of dibutyl phthalate. (B) The binding pocket of CbuqPBP1 and dibutyl  
312 phthalate docked into the active site of the CbuqPBP1 receptor. (C) Diagram of the van der  
313 Waals interactions and hydrophobic interactions of dibutyl phthalate with key binding site  
314 residues.

315 **Figure 3 Double digestion map of the mutant and wild-type plasmids.** Lane Marker: protein  
316 molecular weight standard; Lane 1: pET-28a (+)/PBP1-Phe69A; Lane 2: pET-28a (+)/PBP1-  
317 His53A; and Lane 3: pET-28a (+)/PBP1.

318 **Figure 4 SDS-PAGE analysis of the total bacterial protein lysate of the mutant and wild-**  
319 **type CbuqPBP1.** (A) CbuqPBP1-His53A mutant. Lane 1: IPTG induced total protein lysate;  
320 Lane 2: total protein lysate without IPTG induction. (B) CbuqPBP1- Phe69A mutant. Lane 1:  
321 total protein lysate without IPTG induction; Lane 2: IPTG induced total protein lysate. (C) wild-

322 type CbuqPBP1. Lane 1: IPTG induced total protein lysate; Lane 2: total protein lysate without  
323 IPTG induction.

324 **Figure 5 SDS-PAGE analysis of supernatant and precipitant of bacterial fragmentation**  
325 **following expression of the mutant and wild-type CbuqPBP1.** Lane 1: IPTG induced  
326 expression of insoluble material; Lane 2: IPTG induced expression of supernatant following cell  
327 disruption by sonication. (A) wild-type protein. (B) CbuqPBP1-His53A mutant. (C) CbuqPBP1-  
328 Phe69A mutant.

329 **Figure 6 The binding curve and  $K_d$  of mutant and wild-type CbuqPBP1 toward 1-NPN.** (A)  
330 wild-type protein. (B) CbuqPBP1-His53A mutant. (C) CbuqPBP1- Phe69A mutant.

331 **Figure 7 Competitive binding curves of selected ligands toward mutant and wild-type**  
332 **CbuqPBP1.** (A) wild-type protein. (B) CbuqPBP1-His53A mutant. (C) CbuqPBP1- Phe69A  
333 mutant.

334

## 335 Reference

336 Cavasotto, C.N., and S.S. Phatak. 2009. Homology modeling in drug discovery: current trends and applications.  
337 Drug Discov Today 14: 676-683.

338 Damberger, F.F., Y. Ishida, W.S. Leal and K. Wuthrich. 2007. Structural basis of ligand binding and release in insect  
339 pheromone-binding proteins: NMR structure of *Antheraea polyphemus* PBP1 at pH 4.5. J Mol Biol 373: 811-819.

340 Deng, S.S., J. Yin, T. Zhong and Y.Z. Cao. 2011. Function and immunocytochemical localization of two novel  
341 odorant-binding proteins in olfactory sensilla of the scarab beetle *Holotrichia oblita* Faldermann (Coleoptera:  
342 Scarabaeidae). Chemical Senses 37: 141-150.

- 343 Gu, S.H., S.P. Wang, X.Y. Zhang, K.M. Wu, Y.Y. Guo, J.J. Zhou and Y.J. Zhang. 2011. Identification and tissue  
344 distribution of odorant binding protein genes in the lucerne plant bug *Adelphocoris lineolatus* (Goeze). *Insect*  
345 *Biochem Mol Biol* 41: 254-263.
- 346 Huey, R., G.M. Morris, A.J. Olson and D.S. Goodsell. 2007. A semiempirical free energy force field with charge-  
347 based desolvation. *J Comput Chem* 28: 1145-1152.
- 348 Jiang, Q.Y., W.X. Wang, Z. Zhang and L. Zhang. 2009. Binding specificity of locust odorant binding protein and its  
349 key binding site for initial recognition of alcohols. *Insect Biochem Mol Biol* 39: 440-447.
- 350 Ju, R.T., C.H. Xiao, J.H. Xu, Y. Xu, X.Z. Chi and Y.Z. Li. 2005. *Cyrtotrachelus buqueti* in Shanghai. *Forest Pest and*  
351 *Disease* 24: 7-9.
- 352 Kozmon, S., R. Matuska, V. Spiwok and J. Koca. 2011. Dispersion interactions of carbohydrates with condensate  
353 aromatic moieties: theoretical study on the CH- $\pi$  interaction additive properties. *Phys Chem Chem Phys* 13:  
354 14215-14222.
- 355 Kruse, S.W., R. Zhao, D.P. Smith and D.N. Jones. 2003. Structure of a specific alcohol-binding site defined by the  
356 odorant binding protein LUSH from *Drosophila melanogaster*. *Nat Struct Biol* 10: 694-700.
- 357 Larsson, M.C., A.I. Domingos, W.D. Jones, M.E. Chiappe, H. Amrein and L.B. Vosshall. 2004. Or83b encodes a  
358 broadly expressed odorant receptor essential for *Drosophila* olfaction. *Neuron* 43: 703-714.
- 359 Li, Y.H., P.Y. Deng, Y.M. Liu and Z.H. Lei. 2016. Binding mechanisms of sex pheromone with pheromone binding and  
360 receptor proteins in *Plutella xylostella*. *Journal of Southern Agriculture* 47: 928-933.
- 361 Mang, D.Z., Q.H. Luo, M. Shu and W. Wei. 2012. Extraction and identification of cuticular semiochemical  
362 components of *Cyrtotrachelus buqueti* Guerin-Meneville (Coleoptera: Curculionidae). *Acta Entomol Sin* 55: 291-302.
- 363 Mao, Y., X. Xu, W. Xu, Y. Ishida, W.S. Leal, J.B. Ames and J. Clardy. 2010. Crystal and solution structures of an  
364 odorant-binding protein from the southern house mosquito complexed with an oviposition pheromone. *Proc Natl*  
365 *Acad Sci U S A* 107: 19102-19107.
- 366 Morris, G.M., R. Huey, W. Lindstrom, M.F. Sanner, R.K. Belew, D.S. Goodsell and A.J. Olson. 2009. AutoDock4 and  
367 AutoDockTools4: Automated docking with selective receptor flexibility. *J Comput Chem* 30: 2785-2791.
- 368 Northey, T., H. Venthur, F. De Biasio, F.X. Chauviac, A. Cole, K.A.J. Ribeiro, G. Grossi, P. Falabella, L.M. Field, N.H.  
369 Keep and J.J. Zhou. 2016. Crystal Structures and Binding Dynamics of Odorant-Binding Protein 3 from two aphid  
370 species *Megoura viciae* and *Nasonovia ribisnigri*. *Sci Rep* 6: 24739.
- 371 Sandler, B.H., L. Nikonova, W.S. Leal and J. Clardy. 2000. Sexual attraction in the silkworm moth: structure of the

- 372 pheromone-binding-protein-bombykol complex. *Chem Biol* 7: 143-151.
- 373 Sun, H., L.X. Zhao, F.R. Zhou and H. Gao. 2013. Pheromone binding protein of *Helicoverpa zea* based on Homology  
374 modeling. *Ningxia Journal of Agriculture and Forestry Science and Technology* 54: 37-39.
- 375 Thode, A.B., S.W. Kruse, J.C. Nix and D.N. Jones. 2008. The role of multiple hydrogen bonding groups in specific  
376 alcohol binding site in protein: Insights from structural studies of LUSH. *Journal of Molecular Biology* 376: 1360-  
377 1376.
- 378 Tian, Z.Q., L.N. Sun, Y.Y. Li, H.J. Zhang, W.T. Yan, Q. Yue, L.F. Quan and G.S. Qiu. 2017. Research progress of the  
379 function of sex pheromone binding protein in insects. *Journal of Agriculture* 7: 14-20.
- 380 Vogt, R.G., and L.M. Riddiford. 1981. Pheromone binding and inactivation by moth antennae. *Nature* 293: 161-163.
- 381 Wang, W.D., F.Z. Chen and X.Q. Wang. 2005. Reproductive behavior of *Cyrtotrachelus buqueti*. *Sichuan J Zool* 24:  
382 540-541.
- 383 Wang, Y., H. Sun, J.Y. Zhu, N. Zhao and B. Yang. 2015. Homology modeling of the odorant binding protein of the  
384 pine shoot beetle, *Tomicus yunnanensis*. *Chinese Journal of Applied Entomology* 54: 1223-1228.
- 385 Yang, H., T. Su, W. Yang, C. Yang, L. Lu and Z. Chen. 2017a. The developmental transcriptome of the bamboo snout  
386 beetle *Cyrtotrachelus buqueti* and insights into candidate pheromone-binding proteins. *PLoS One* 12: e0179807.
- 387 Yang, H., T. Su, W. Yang, C.P. Yang, Z.M. Chen, L. Lu, Y.L. Liu and Y.Y. Tao. 2017b. Molecular characterization,  
388 expression pattern and ligand-binding properties of the pheromone-binding protein gene from *Cyrtotrachelus*  
389 *buqueti*. *Physiol Entomol* 42: 1-10.
- 390 Yang, H., T. Su, W. Yang, C.P. Yang, X.L.Zhou and Y. P. Li 2018. Molecular Cloning and Expression Analysis of  
391 CbuqPBP1 Gene in the Bamboo Snout Beetle, *Cyrtotrachelus buqueti*. *Journal of Sichuan Agricultural University*  
392 36:78-85.
- 393 Yang, H., W. Yang, C.P. Yang, Y. Cai, Y.F. Pu, Y.W. Fu and Z.R. He. 2015. Mating behavior of *Cyrtotrachelus buqueti*  
394 (Coleoptera: Curculionidae). *Acta Entomol Sin* 58: 60-67.
- 395 Yang, Y.J., H. Qin, S.F. Wang, Y.P. Wang, H. Liao and S.G. Li. 2010. Antennal ultrastructure and electroantennogram  
396 responses of *Cyrtotrachelus buqueti* Guerin-Meneville (Coleoptera: Curculionidae) to volatiles of bamboo shoot.  
397 *Acta Entomol Sin* 53: 1087-1096.
- 398 Yang, Y.J., S.F. Wang, J.W. Gong, C. Liu, C. Mu and H. Qin. 2009. Relationships among *Cyrtotrachelus buqueti* larval  
399 density and wormhole number and bamboo shoot damage degree. *Chinese J Appl Ecol* 20: 1980-1985.
- 400 Ye, Y.X., J.J. Liang, H.P. Wang, Z. Meng, X.D. Zhang and L.X. Xu. 2015. Noncovalent surface functionalization of

401 multi-walled carbon nanotubes with polyhedral oligomeric silsesquioxane nanoparticles based on CH- $\pi$   
402 interactions. Acta Polymerica Sinica 4: 427-436.

403 Zhao, C., P. Li, M.D. Smith, P.J. Pellechia and K.D. Shimizu. 2014. Experimental study of the cooperativity of CH- $\pi$   
404 interactions. Org Lett 16: 3520-3523.

405 Zhuang, X., Q. Wang, B. Wang, T. Zhong, Y. Cao, K. Li and J. Yin. 2014. Prediction of the key binding site of odorant-  
406 binding protein of *Holotrichia oblita* Faldermann (Coleoptera: Scarabaeida). Insect Mol Biol 23: 381-390.

407 Zhuang, X.J., J. Yin, K.B. Li and Y.Z. Cao. 2013. Bioinformatics analysis of the odorant-binding protein HobLOBP2 in  
408 olfactory sesilla of the scarab beetle *Holotrichia oblita*. Plant Protection 39: 50-55.

409

410

**Table 1** (on next page)

Mutagenic primers for CbuqPBP1

Primers	Sequence
PBP1-F69A-Fm	5'-aatgcactatctgtacagcgaaaaattcgattgatgaaag-3'
PBP1-F69A-Rm	5'-ctttcatcaaatcgaatcttcgctgtacagaaaatagtcatt-3'
PBP1-H53A-Fm	5'-gatatccaagctctgatgaacgcggaacgaccagtcacccatgc-3'
PBP1-H53A-Rm	5'-gcatgggtgactggctcgtccgcgttcacagagcttgatc-3'
PBP1-F	5'-ggaattccatagcttagcgaagcttagttgtgatg-3'
PBP1-R	5'-ccgctcgagttaaaaactgtaattccaag-3'

1

2

**Table 2** (on next page)

Binding ability of ligands to mutant and wild-type CbuqPBP1

Ligands	IC50 ( $\mu\text{M}$ )			Ki ( $\mu\text{M}$ )		
	PBP1	H53A	F69A	PBP1	H53A	F69A
benzothiazole	13.426	–	10.538	9.822	–	7.305
dibutyl phthalate	16.889	–	20.04	12.355	–	13.893
cedrol	29.953	–	–	21.912	–	–

1

2

# Figure 1

Three-dimensional (3D) model of CbuqPBP1

(A) Sequence alignment between CbuqPBP1 and NribOBP3. (B) 3D structure of CbuqPBP1. The N and C termini and the six  $\alpha$ -helices are labeled and the three disulfide linkages are shown in yellow stick representations. (C) Superimposed penetrative structure of CbuqPBP1 and NribOBP3. The model of CbuqPBP1 and crystal structure of NribOBP3 are shown in green and violet, respectively. (D) The results of the PROCHECK evaluation of the CbuqPBP1 model. (E) Overall model quality.

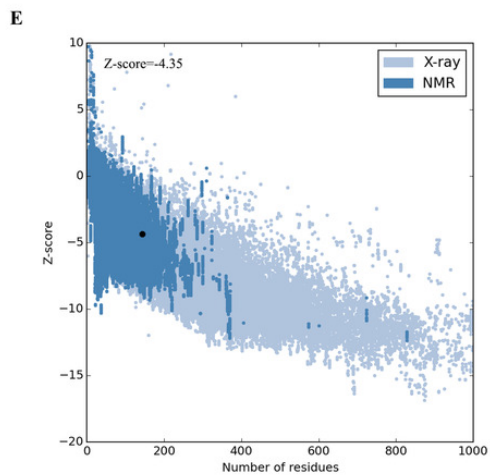
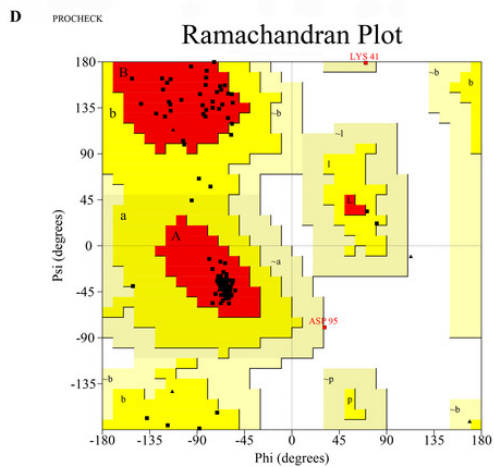
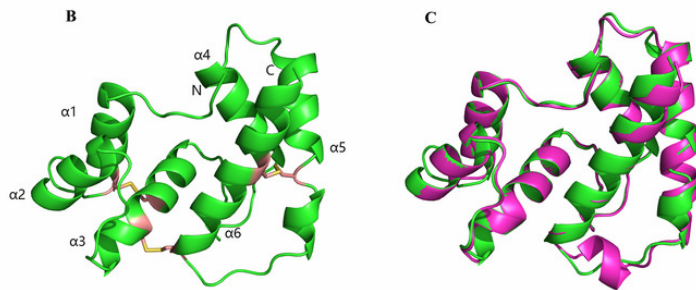
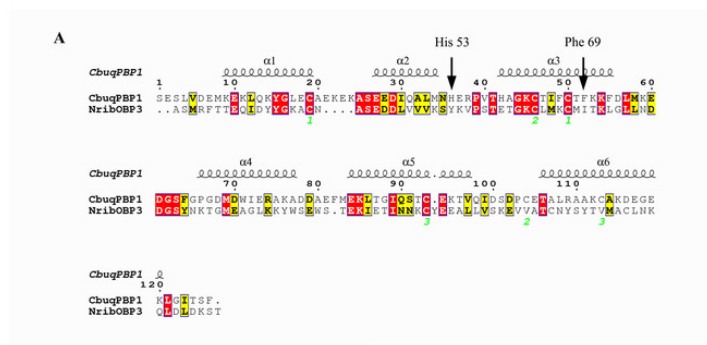
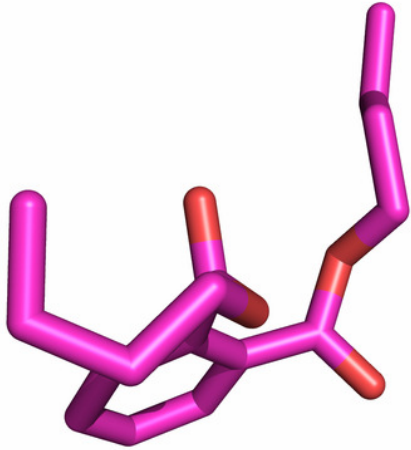


## Figure 2

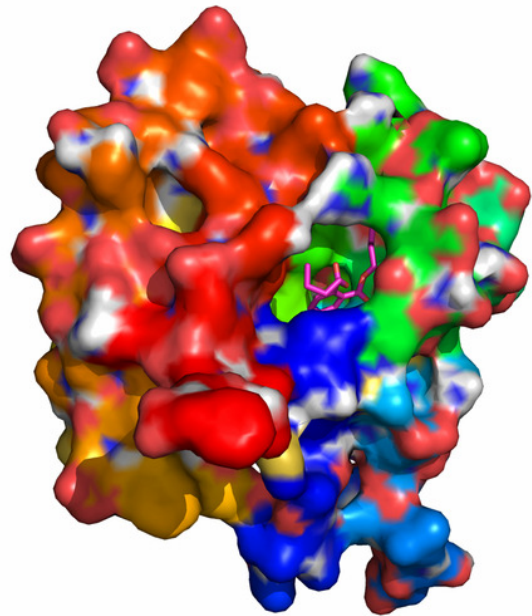
The binding pocket of CbuqPBP1 and the docking result with dibutyl phthalate

(A) Tertiary structure of dibutyl phthalate. (B) The binding pocket of CbuqPBP1 and dibutyl phthalate docked into the active site of the CbuqPBP1 receptor. (C) Diagram of the van der Waals interactions and hydrophobic interactions of dibutyl phthalate with key binding site residues.

A



B



C

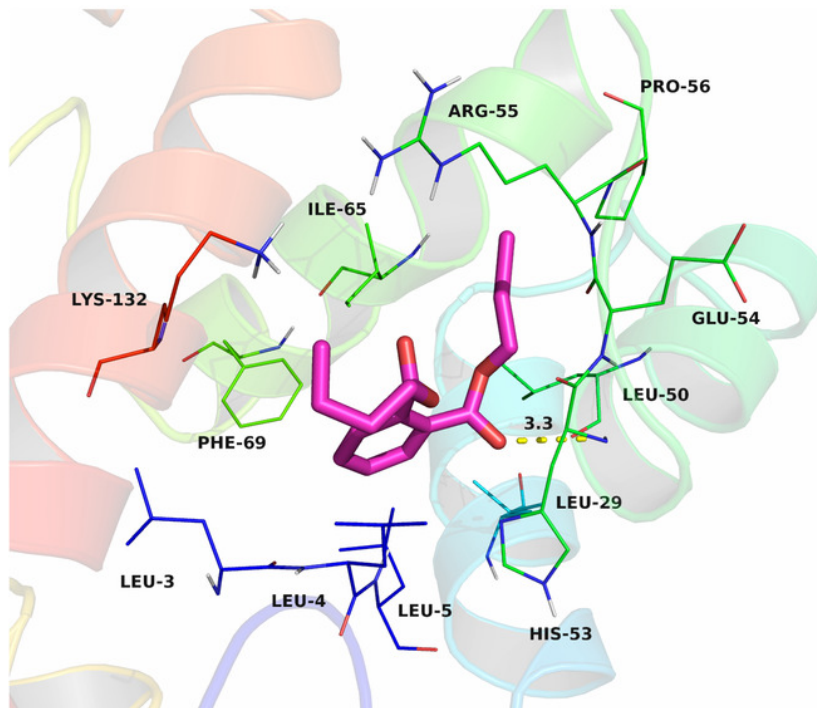


## Figure 3

Double digestion map of the mutant and wild-type plasmids

Lane Marker: protein molecular weight standard; Lane 1: pET-28a (+)/PBP1-Phe69A; Lane 2: pET-28a (+)/PBP1-His53A; and Lane 3: pET-28a (+)/PBP1.

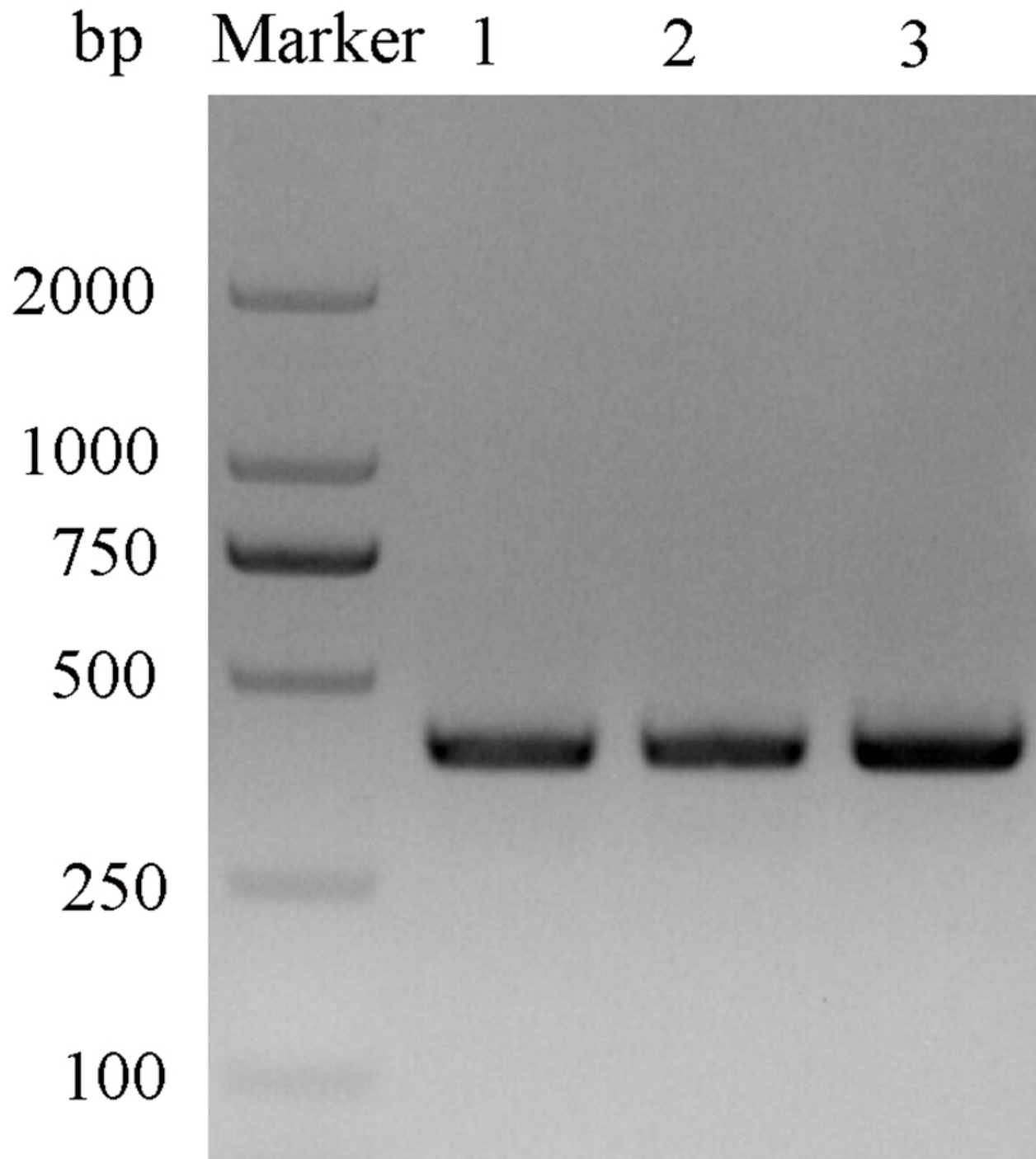


## Figure 4

SDS-PAGE analysis of the total bacterial protein lysate of the mutant and wild-type CbuqPBP1

(A) CbuqPBP1-His53A mutant. Lane 1: IPTG induced total protein lysate; Lane 2: total protein lysate without IPTG induction. (B) CbuqPBP1- Phe69A mutant. Lane 1: total protein lysate without IPTG induction; Lane 2: IPTG induced total protein lysate. (C) wild-type CbuqPBP1. Lane 1: IPTG induced total protein lysate; Lane 2: total protein lysate without IPTG induction.

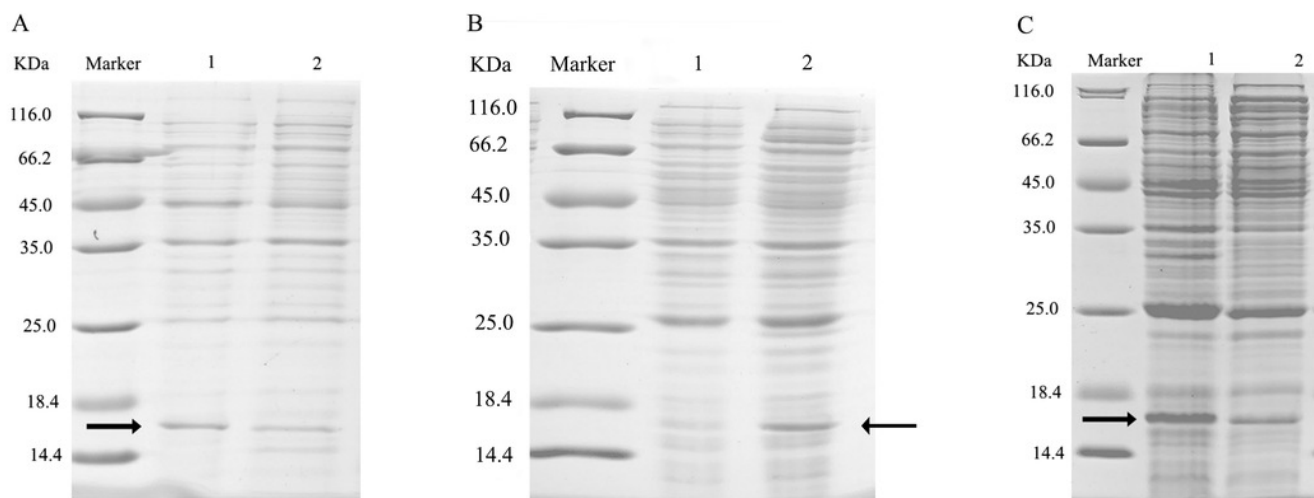


## Figure 5

SDS-PAGE analysis of supernatant and precipitant of bacterial fragmentation following expression of the mutant and wild-type CbuqPBP1

Lane 1: IPTG induced expression of insoluble material; Lane 2: IPTG induced expression of supernatant following cell disruption by sonication. (A) wild-type protein. (B) CbuqPBP1-His53A mutant. (C) CbuqPBP1- Phe69A mutant.

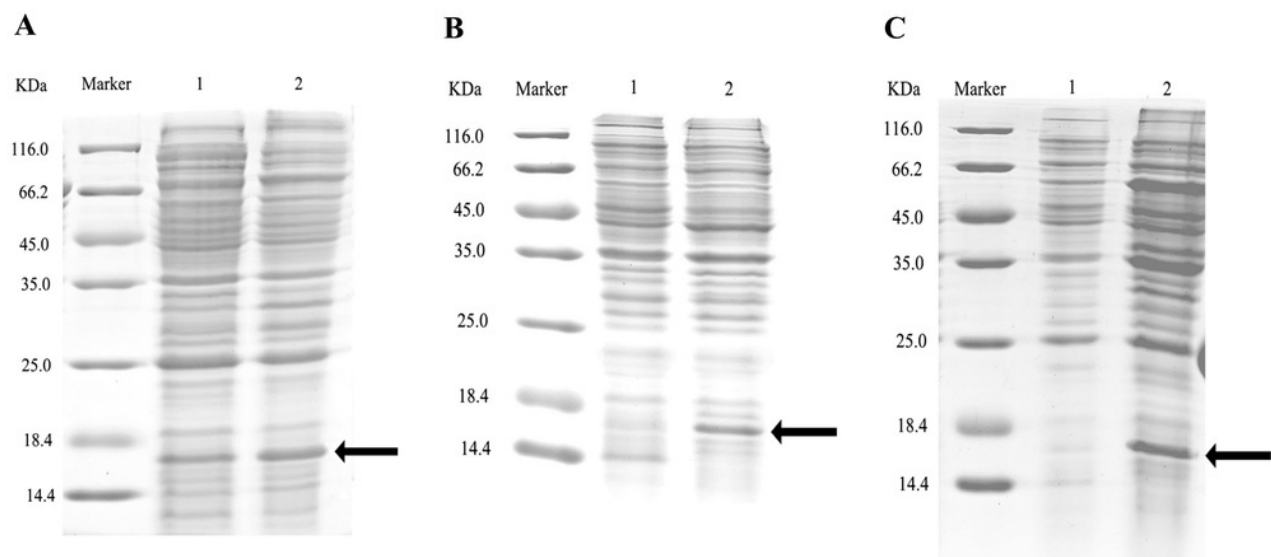
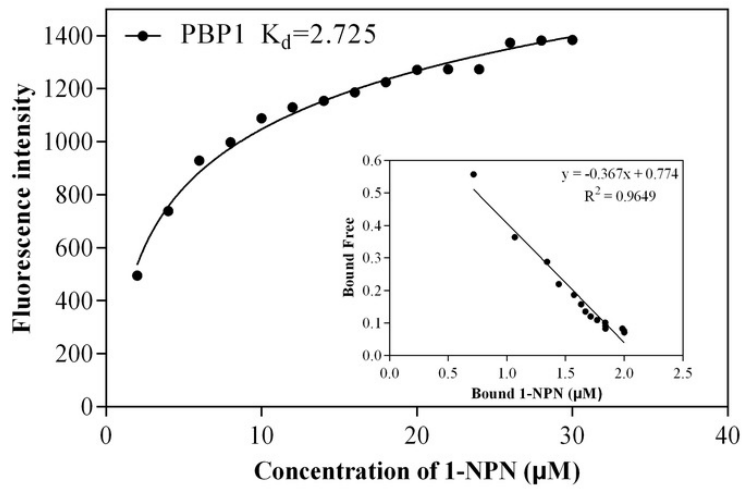


## Figure 6

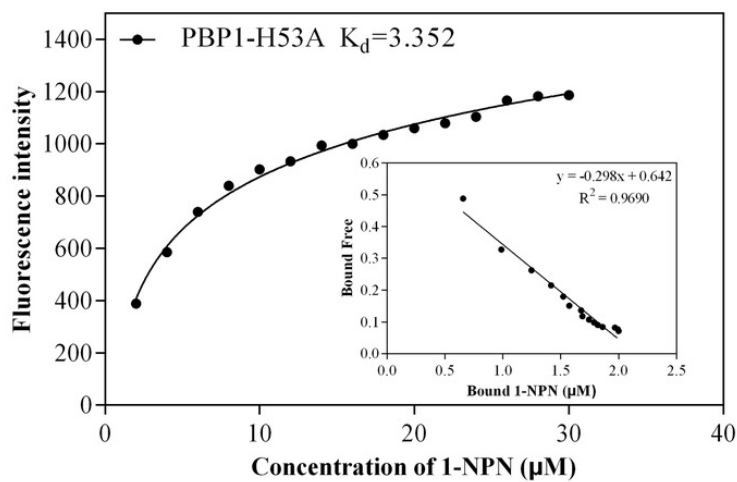
The binding curve and  $K_d$  of mutant and wild-type CbuqPBP1 toward 1-NPN

(A) wild-type protein. (B) CbuqPBP1-His53A mutant. (C) CbuqPBP1- Phe69A mutant.

A



B



C

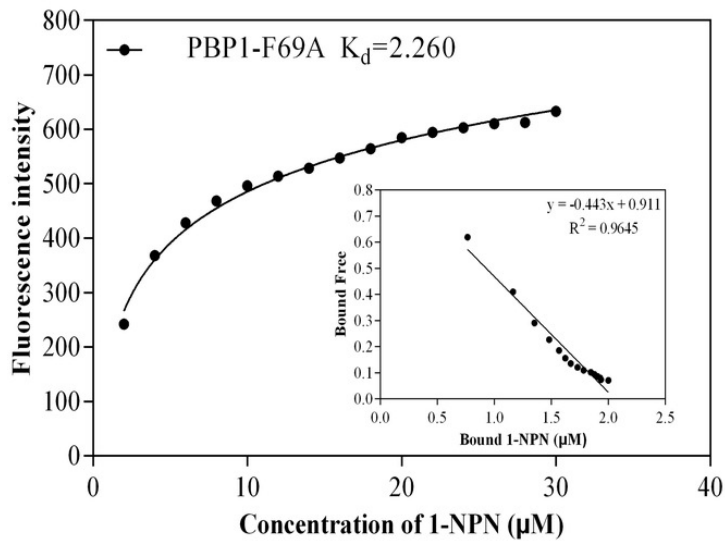


## Figure 7

Competitive binding curves of selected ligands toward mutant and wild-type CbuqPBP1

(A) wild-type protein. (B) CbuqPBP1-His53A mutant. (C) CbuqPBP1- Phe69A mutant.

